Additive Manufacturing 32 (2020) 100975

Contents lists available at ScienceDirect

Additive Manufacturing

journal homepage: www.elsevier.com/locate/addma

Full Length Article

Conformal additive manufacturing using a direct-print process

Faez Alkadi[a,b], Kyung-Chang Lee[c], Abdullateef H. Bashiri[b], Jae-Won Choi[a,c,*]

[a] The Department of Mechanical Engineering, The University of Akron, 244 Sumner Street, Akron, OH, 44321, USA
[b] The Department of Mechanical Engineering, Jazan University, Jazan, 45142, Saudi Arabia
[c] Department of Control and Instrumentation Engineering, Pukyong National University, Busan, 48513, Republic of Korea

ARTICLE INFO

Keywords:
Material extrusion
Conformal additive manufacturing
Freeform substrate
Direct-print
Freeform slicing

ABSTRACT

In conventional additive manufacturing, most processes for creating the layers of a part are performed on a horizontal plane. In contrast, a conformal additive manufacturing process has been suggested in order to build a real 3D structure on a freeform surface using a direct-print process based on material extrusion. A new algorithm was developed that is able to use the standard 3D printing file format that includes both a 3D model to be printed and a 3D model of a freeform substrate along with the desired printing parameters as input, and it returns G-code instructions for the 3D printing process as output. A slicing surface was generated to slice the 3D model by offsetting the surface of a freeform substrate model by a discrete amount (i.e., layer thickness) for each layer. The perimeters of each layer (including the internal features) were extracted based on the intersections between the slicing surface and the 3D model, and infill toolpaths were created by projecting 2D patterns reflecting the features to be printed with a desired fill factor (in the x–y plane) onto the slicing surface to create 3D patterns. Two printing methods, complete conformal printing and a hybrid methodology that combines conformal printing with conventional horizontal printing, were presented. Several 3D models were sliced and printed on a freeform surface to validate the developed algorithm.

1. Introduction

Additive manufacturing is the technology where three-dimensional (3D) objects can be horizontally sliced and built in a layer-by-layer fashion; thus, it is also known as *3D printing* [1]. Additive manufacturing technology can be divided into three major processes based on material types: liquid-based, solid-based and powder-based, where each process has one or more sub-processes [1,2]. Fused filament fabrication (FFF) is a liquid-based process where a molten, liquid or paste material leaves a printing nozzle in a filament form [1,3,4]. This process can be used to print structures made either from a single material [5–10] or from multiple materials [11–14] by controlling the process parameters (e.g., material flow rate and printing speed) of an extruder. Filament-based processes can be used for printing structures on flat surfaces [4,15–17] or freeform (non-planar) surfaces [18–23]. Moreover, a wide range of functional [15–17,22,24] or prototyping [2,3,25–28] inks can be utilized in such processes.

Quality of 3D printed parts can be evaluated based on multiple factors such as mechanical properties and the level of surface finish. Mechanical properties are mainly based on material properties and filament-related factors such as printing angle and infill density [14,28,29]. The quality of the surface finish depends on the layer thickness, which generally produces a stair-step effect that results from layer-wise fabrication. Research on FFF processes has been conducted with the aim of improving the mechanical properties [25,30–32] and surface finish [28,33] of 3D printed parts. Planar slicing and layering in the 3D printing processes can yield poor mechanical properties and surface finish, which result from the weak interconnection between layers and the stair-step effect. Conformal additive manufacturing, a 3D printing process for printing a 3D structure on a freeform surface in which slicing and layering are conducted, has been suggested as a potential method to overcome these problems. In conventional additive manufacturing, called *planar additive manufacturing*, the z-value (i.e., the coordinate on the z-axis of a Cartesian coordinate system) does not change in a single layer. In contrast, in conformal additive manufacturing, the z-axis coordinate continuously changes in the same layer, depending on the complexity and topology of a slicing surface. Freeform FFF processes have been introduced to resolve only a single thin and curved layer (that is concave and/or convex) [34] or multiple but duplicated initial layers to achieve higher strength due to the presence of continuous filaments [18–21,35]; these processes are able to improve the surface finish by partially eliminating the stair-step effect and, to some extent, have also decreased the build time required for printing a part.

* Corresponding author at: The Department of Mechanical Engineering, The University of Akron, 244 Sumner Street, Akron, OH, 44321, USA.
E-mail address: jchoi1@uakron.edu (J.-W. Choi).

https://doi.org/10.1016/j.addma.2019.100975
Received 25 June 2019; Received in revised form 8 October 2019; Accepted 25 November 2019
Available online 27 November 2019

Challenges facing conformal additive manufacturing are related to material properties and the algorithm used to generate the toolpath. Rheological properties play a key role in creating layers accurately for both planar [7,17,36] and freeform [37] processes in addition to printing speed, curing time and gap height [7,8,37]. To overcome some of these challenges, Jacob et al. [22] used different nozzles and adjusted the tip angle. As generating an accurate toolpath is one of the biggest challenges for conformal additive manufacturing, some research has focused on this aspect. Singamneni et al. [18] used two approaches to extract data points for a layer from the top surface of the part: one approach is to process data from a computer-aided manufacturing (CAM) module, and the other is to use data in an STL format from a slicing model with a vertical slicing surface to generate surface data points. Allen et al. [20] used a surface equation to calculate z values after converting the surface to an array of data points in the *x–y plane* over a grid having the same size as the surface and using a resolution equal to the desired distance between the printed filament lines. Yuan et al. [35] extracted toolpath data points from a tessellated surface after fitting it into a B-spline, where the first path is chosen on the design surface along one of its edges and the next path will be calculated accordingly until the ending edge for the layer. From studies published in the literature, it can be noticed that there is lack of agreement regarding the practical generation of a toolpath for 3D printing of arbitrary structures on freeform surfaces [18,20,21,34,35].

In this work, conformal 3D printing algorithms were developed and used for building arbitrary 3D structures on freeform substrates. The proposed algorithms generate data points for each layer in order to build a 3D structure according to the topology of the freeform substrate. The data points are generated based on the desired printing parameters (nozzle size, gap height, fill density, etc.). As a result, the nozzle toolpaths are generated by taking into consideration the change in the angle between the printing nozzle and the freeform substrate.

2. Conformal 3D slicing algorithm

The printing head in extrusion-based 3D printing moves according to tool path data points distributed in the Cartesian space (i.e., the *x, y,* and *z* axes). In planar 3D printing, a filament is deposited in the *x–y* plane within the same layer, while the *z*-value is constant in each layer with an amount equal to the desired layer thickness. In contrast, for conformal 3D printing, the *z*-value changes dynamically with *x–y* values within the same layer according to the shape of the freeform substrate. Toolpath planning depends on the perimeters and the fill pattern defined for each layer. A flowchart showing the entire processes including the extraction of the toolpath data points for both the perimeters and the infill areas to realize conformal 3D printing is presented in Fig. 1. It is noted that pseudo codes for all the algorithm in the following sections are provided in Supplementary Information.

2.1. Generating toolpaths for direct printing in a single layer

In this study, a novel algorithm was developed to generate toolpaths for the conformal additive manufacturing process for 3D printing of a structure on a freeform surface:

2.1.1. Step 1: prepare and Load the substrate model (freeform surface) and the 3D model for the part to be printed

The first step in the toolpath generation algorithm for conformal 3D printing is to identify the surface of the freeform substrate. Surface information for an unknown freeform substrate can be easily obtained and reconstructed by using a 3D laser scanner, which can generate a point cloud [38]. Another method is to use computer-aided design (CAD) software to create a freeform substrate model as a pre-designed part, as was the case in this study.

A 3D model can be designed and placed on a freeform surface using an *assembly* feature in a CAD program such as SolidWorks (Fig. 2b). Combining the 3D model and the freeform surface will result in two possible scenarios: either the bottom of the 3D model fits the freeform surface or it does not. If the bottom of the model fits the freeform surface (as shown in Fig. 2b), both the model and the freeform surface can be imported to the slicing algorithm in their as-is forms. However, if the bottom of the model does not fit the freeform surface (as shown in Fig. 2c), two methods can be used to join the two parts and obtain the proper fit. In the first fitting method, the 3D model is modified so that the bottom of the printed part extends to the freeform surface using the *Extrusion* feature in the CAD software. The result for this method will be a new 3D model (henceforth referred to as the *modified 3D model*) (as shown in Fig. 2d), and the slicing method will be fully conformal from bottom to top (as explained later in this section), where the inputs for this method are the two objects (the freeform surface and the modified 3D model). In the second fitting method, which is used for cases where the printed part is not editable, a new piece called a *base* is built between the 3D model and the freeform surface (as shown in Fig. 3b). The base is generated with its top matching (fitting) with the 3D model and its bottom matching (fitting) with the freeform substrate, so it fills the gap between the 3D model and the freeform substrate. Consequently, a hybrid slicing technique (which will be described in detail in Section 2.2) will be applied, where the input includes three pieces: the freeform surface, the base and the 3D model. For both fitting methods, data for all pieces must be translated into STL format to be compatible with the proposed slicing algorithm.

In this study, the hexagonal part shown in Fig. 3a, b will be used as an example to explain the proposed 3D slicing algorithm in greater detail. Following this explanation, the proposed slicing algorithm will subsequently be applied to more complex models to demonstrate its universality.

2.1.2. Step 2: determine the offset of the freeform substrate to be used as a slicing surface

A gap height (the distance between printing substrate and the nozzle tip) is one of the main factors having a direct influence on the filament shape and printing quality. In conventional planar printing using a Cartesian 3D printing system (one that uses an XYZ-stage), the gap height can be set by moving the substrate (or printing nozzle) vertically by an amount H (where H = layer thickness × layer number) for each layer. For conformal printing, in contrast, the gap height should always be fixed according to the normal of the surface of the freeform substrate. Thus, in this study, an offset surface (slicing surface) (Fig. 4a) with the normal direction throughout the surface of the freeform substrate was generated with an offset amount equal to the desired gap height (H). This normal offset was applied to maintain a constant normal distance between the freeform substrate and the tool path data points for each layer. The constant distance between the tool path and the freeform surface ensures that the distance between the middle of the nozzle tip and the surface of the freeform substrate will be constant throughout the whole layer.

In generating the slicing surface (Fig. 4a), the *gptoolbox* function in MATLAB (MathWorks, Natick, Mass.) was used to handle the input data in STL format. The slicing surface for each layer is an offset form of the freeform surface with the appropriate offset distance (H). The generated slicing surface is used to slice the 3D model for the part in a comfortable manner and extract the data points for the tool path, as explained in the following step.

2.1.3. Step 3: extract the perimeters for the toolpath

Since the slicing surface and the 3D model both consist of triangles (as the STL file divides the surface of a 3D object into small triangles having vertices and faces), the triangle/triangle intersection algorithm was applied [40]. Fig. 5a shows the intersection of two surfaces (Surface 1 from the slicing surface and Surface 2 from the 3D model), in which each surface consists of the faces of two triangles. The result of this intersection is an edge (shown in red in Fig. 5a) that is divided into

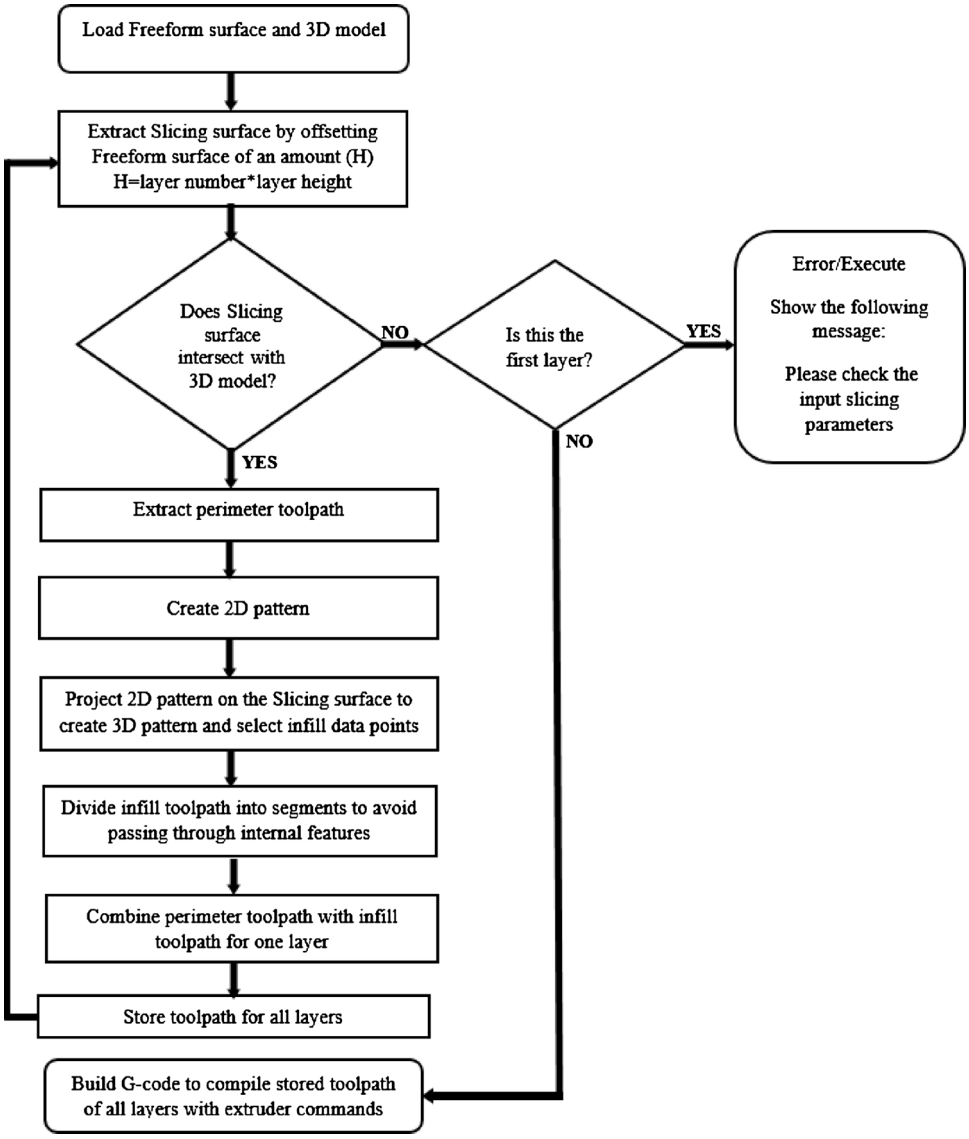

Fig. 1. Flowchart for the algorithm used in conformal 3D slicing.

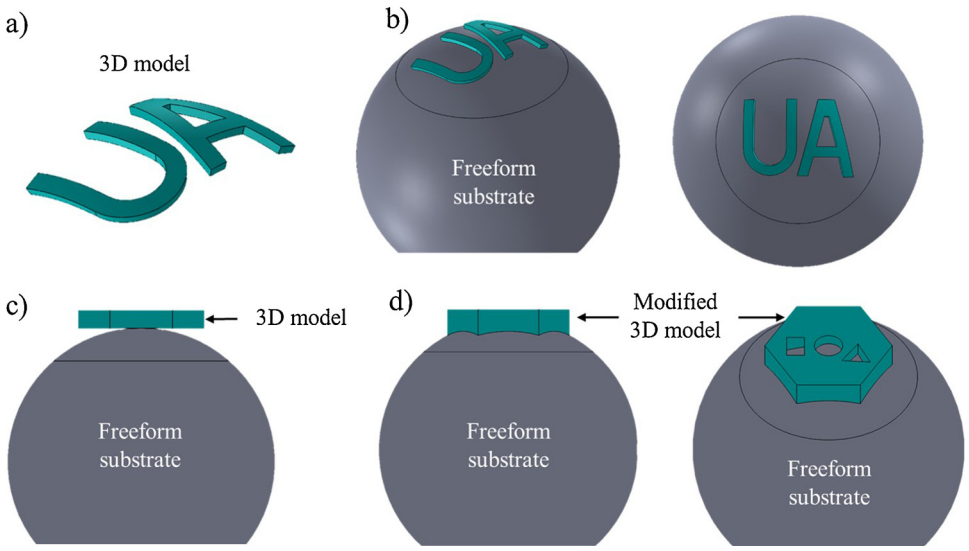

Fig. 2. CAD models for the freeform substrate and the desired part created in SolidWorks: a) 3D model for a part to be printed on a spherical freeform substrate; b) 3D view and top views of the model as placed on the substrate; c) Side view of an original 3D model as placed on the substrate; and d) Side and top views of the modified 3D model as placed on the substrate.

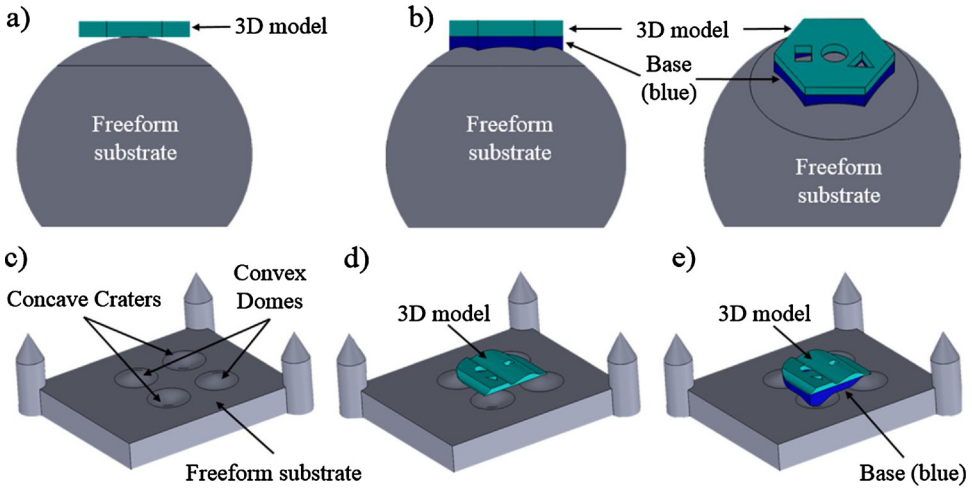

Fig. 3. CAD models for freeform substrates and 3D models for the desired parts using SolidWorks: a) 3D model of desired part to be printed (shown in green) on a spherical freeform substrate; b) Fitting the part with the substrate by adding a new piece called a *base* (shown in blue); c) A complex freeform substrate with flat, concave and convex surfaces; d) An arbitrary-shaped printed part placed on a complex freeform substrate; and e) Fitting the printed part with the freeform surface by adding a base. (For interpretation of the references to colour in this figure legend, the reader is referred to the web version of this article.)

three segments, where each segment represents the intersection between a specific triangle on the slicing surface and a specific triangle on the 3D model surface.

As a result, in the proposed algorithm, the intersection lines (edge segments) where each triangle (face) on the slicing surface intersects with a triangle (face) in the 3D model (as shown in Fig. 4a) were used as the perimeters and the internal feature of the current layer (shown in Fig. 4b). These lines are post-processed and organized to be projected as a ray in a single direction (either in the clockwise or the counter-clockwise direction, according to the x–y plane) from the origin point that is used for the tool path.

2.1.4. Step 4: create data points for 2D infill patterns

Infill pattern data points are created in 2D (the *x*–*y* plane), as shown in Fig. 4c, and will be projected on the slicing surface for each layer in order to extract the 3D infill pattern data points for the layer (Fig. 4d). In this work, the 2D pattern (in the *x*–*y* plane) is presented in a zigzag shape (0^o and 90^o to the *x*-axis) for the sake of simplicity, although any

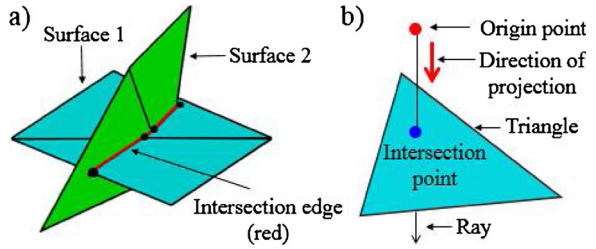

Fig. 5. Diagrams showing the geometry of the slicing algorithm: a) Triangle-to-triangle intersection, where Surface 1 is from the slicing surface (shown in cyan) and Surface 2 is from the 3D model (shown in green); and b) Ray-to-triangle intersection of one point from 2D pattern (red) on one triangle on the slicing surface. (For interpretation of the references to colour in this figure legend, the reader is referred to the web version of this article.)

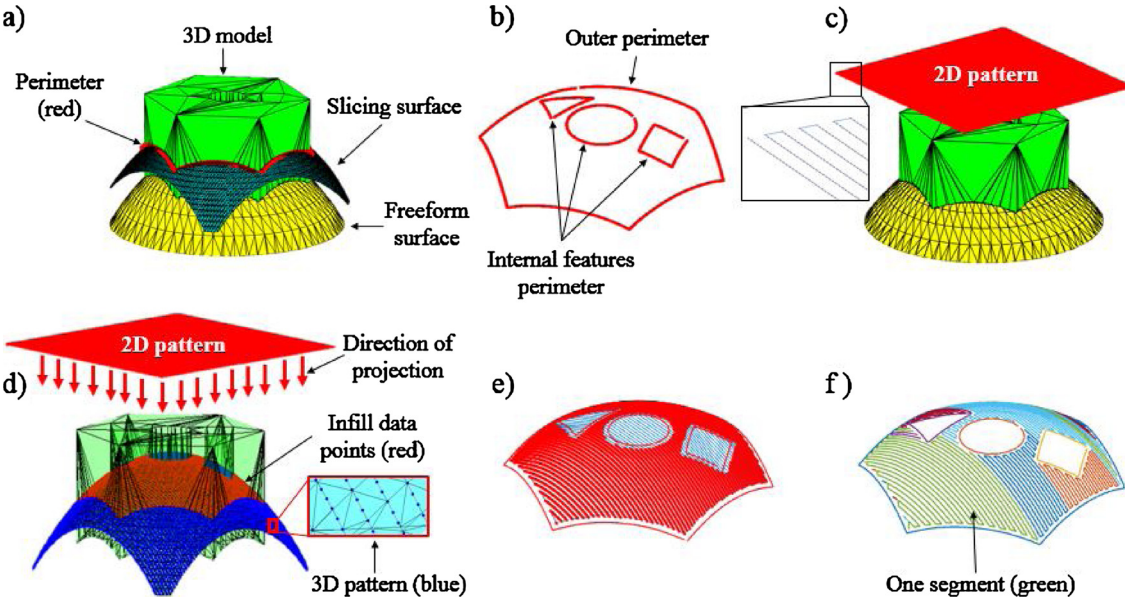

Fig. 4. Steps for generating toolpath for one layer after saving CAD models in STL format: a) Generating the slicing surface by offsetting freeform surface by an amount H (where H = layer number × gap height) and finding the layer perimeters (the intersection between the slicing surface and the printed part); b) Perimeters for one layer; c) Generating the 2D pattern for the infill data points; d) Projecting the 2D pattern on the slicing surface and extracting the 3D pattern (shown in blue) and finding the infill data points (shown in red); e) Combining the perimeters and infill data points to find the toolpath for one layer; f) Dividing the tool path into segments to prevent the path from passing through internal features of the layer during 3D printing. (For interpretation of the references to colour in this figure legend, the reader is referred to the web version of this article.)

pattern could potentially be applied. The 2D zigzag pattern was designed according to the printing parameters (specifically, the nozzle size and fill density) using MATLAB (Fig. 4c).

2.1.5. Step 5: create data points for 3D infill patterns and select infill data points

After extracting the perimeters for each layer, the 2D pattern data points from Step 4 are projected on the slicing surface to create 3D pattern data points according to the shape of the slicing surface (Fig. 4d-blue), and accordingly, infill data points are selected (Fig. 4d-red). To obtain the 3D pattern, the projection algorithm of the 2D pattern on the slicing surface was established based on the ray/triangle intersection algorithm [41]. Fig. 5b shows the result for a projection of one data point (shown as a blue dot on the face) from a point on the 2D pattern (shown as a red dot above the plane of the face) for a single triangle face of the slicing surface using the ray/triangle intersection algorithm. The 3D infill pattern is the result of applying this algorithm to all points on the 2D pattern for every face on the slicing surface. From the data points for the 3D pattern (shown in blue in Fig. 4d), only the data points inside the polyhedron (shown in red in Fig. 4d) are selected as infill data points.

2.1.6. Step 6: combine the perimeters and the infill data points of one layer and divide it into segments

The layer perimeters of the outer wall and the internal features from Step 3 will be combined with the infill data points from Step 5 in order to extract the final toolpath for each one layer (Fig. 4e). An algorithm was developed to prevent the toolpath from passing through the internal features of the layer while printing the infill material. This algorithm divides the infill pattern data points into several segments (Fig. 4f) so that in the G-code required for printing each layer, start and stop commands for material flow can be added before and after each subsequent segment.

In a previous publication [39], the authors demonstrated that an effective gap height in conformal printing is the distance between the back edge of the nozzle tip (according to the direction of motion) and the freeform surface. This distance changes dynamically according to the angle between the normal of the substrate and printing nozzle (on the z-axis). In order to maintain the effective gap height during conformal printing, the authors successfully developed an algorithm and conducted experiments to verify it [39]. Therefore, in this work, the developed algorithm was applied on the data points of every single segment of the perimeters and the infill to maintain the effective gap height for the entire layer.

2.1.7. Step 7: repeat steps 2 through 6 until all layers are considered

After extracting the tool path for one entire layer (perimeters and infill segments), the toolpath for that layer is stored, and Steps 2 through 6 are repeated in order to obtain the tool path for the next layer. It should be noted that the gap height, H, increases with the increase in the layer number, as shown in Fig. 6a, b. This loop continues until no intersection exists between the slicing surface and the 3D model Fig. 6c.

2.1.8. Step 8: import stored data points for tool path segments into an algorithm to generate the G-code

Once the slicing surface reaches beyond the 3D model, where no intersection exists between the slicing surface and the 3D model (Fig. 6c), the stored data points of tool path segments for all layers are imported into an algorithm, where the G-code for the entire printing process can be generated. In the generated G-code, the printing parameters (printing speed, material flow rate, and material extrusion start/stop command) are synchronized with every segment in each layer in order to build the entire part.

2.2. Hybrid slicing method

In the previous method (fully conformal slicing from the bottom to the top of the 3D model), the 3D model and the base (Fig. 3b) were both combined and conformably sliced as a single part from bottom to top (Fig. 6a, b). In the hybrid slicing method, both the conformal and conventional planar slicing methods are combined. The base (shown in blue in Fig. 7a) is sliced conformably, as in the first method (Fig. 6b). As a result, the top of the base becomes flat and has the same surface shape as the desired part. Next, the 3D model (shown in green in Fig. 7a) is sliced conventionally in planar 2D layers using a 2D slicing surface (shown in magenta in Fig. 7a). Finally, both the conformal and planar layers of the base and the printed part, respectively, are combined into a series of G-code instructions that build both pieces as a single part (Fig. 7b).

3. Experiments

3.1. Materials used for the model and substrate

3D printable materials with controlled rheological properties were developed to be used as a printing ink to demonstrate the capability of the proposed algorithm to build 3D structures on freeform surfaces. The printable ink was prepared by mixing TangoPlus FullCure® 930 resin (Stratasys, Eden Prairie, Minn., USA) as the main material, with 10 wt% of M-5 CAB-O-SIL® fumed silica (Cabot Corp., Billerica, Mass., USA), to introduce a thixotropic property to the ink. The thixotropic property of the ink is important, as it helps the ink maintain its filament shape after it leaves the nozzle and prevents the ink from spreading, enabling the printed part to remain in a gel-like state. The mixing process was performed in a FlackTek SpeedMixer™ high-speed mixer (Landrum, SC, USA) with the addition of mixing beads at 2500 rpm for 5 min.

3.2. Printing system

A customized direct-print (DP) system previously developed at The University of Akron was used to print the developed inks [39]. The system, shown in Fig. 8, consists of a Nordson Ultimus™ pressure controller (East Providence, RI, USA) and a Aerotech PRO115 motorized XYZ linear stage (Pittsburgh, PA, USA), with a syringe installed on the Z-stage. The pressure controller and the XYZ linear stage were synchronized using G-code instructions in Aerotech control interfaces and LabVIEW. For the freeform substrate, a sphere made of Grade 25 chrome steel (G25) with a diameter of 76.2 mm was used.

3.3. Conformal 3D printing process

The G25 sphere used as a freeform substrate was fixed to the XY-stage (Fig. 8a, b) using three sharp tapered cylinders fixed at a known distance from the sphere (according to the dimensions of the stage tabletop). These cylinders were used as a registration reference to find the origin point ($x = 0$, $y = 0$, $z = 0$) for a coordinate system on the surface of the sphere (as shown in Fig. 8b). A 0.335-mm nozzle was used to print a hexagonal part in this experiment, which yielded a 100 % gap height of 0.335 mm and, accordingly, a 0.335-mm layer offset was applied for the desired shape in the CAD model. Raster angles of 0° and 90° were used for the odd layers and even layers, respectively, of the hexagonal part printed in this experiment. Some internal features (such as circular, triangular, and square shapes as shown in Fig. 4b) were added to the design of the printed part to verify the ability of the algorithm to 3D slice and print any 3D object on a freeform surface. All models were 3D-printed with the speed of 15 mm/s.

For the purpose of showing the universality of the developed process, a freeform surface with a complicated topology (as shown in Fig. 3c) was designed to be used as a substrate. The model to be printed was placed on the designed substrate surface (Fig. 3d) and a base was

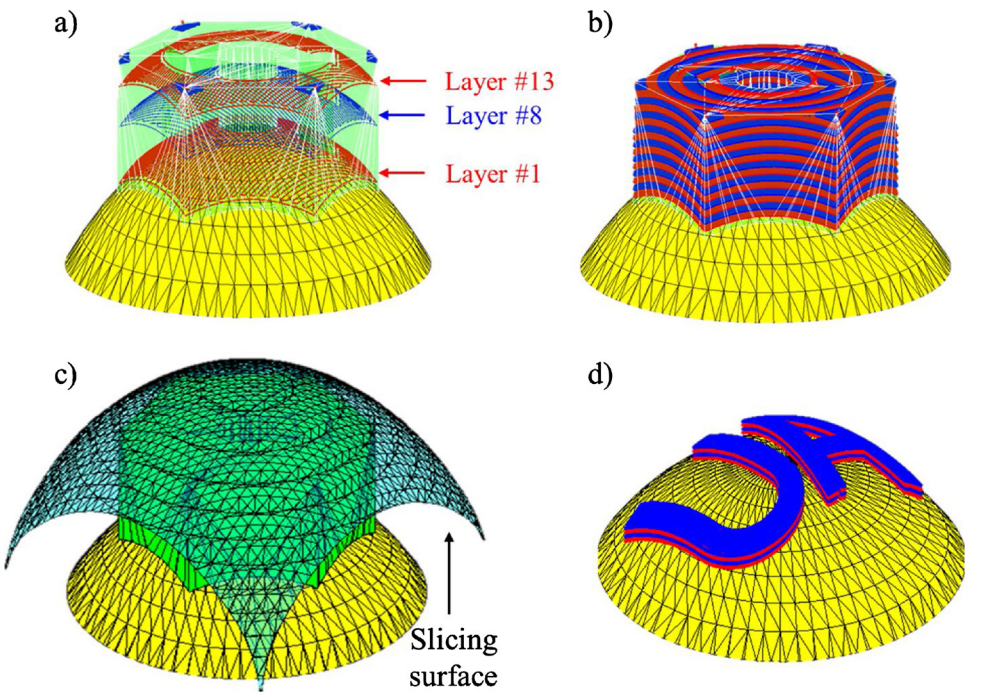

Fig. 6. Visual representation of the printing layers of a hexagonal-shaped part with internal features: a) 3D view showing some of the layers; b) 3D view of all layers needed for building the part, c) 3D view of the slicing surface (shown in cyan) extending beyond the 3D model, where no intersection with the 3D model exists and the execution of the slicing process is ended; and d) 3D view of all layers needed for building the UA model in Fig. 2a, b.

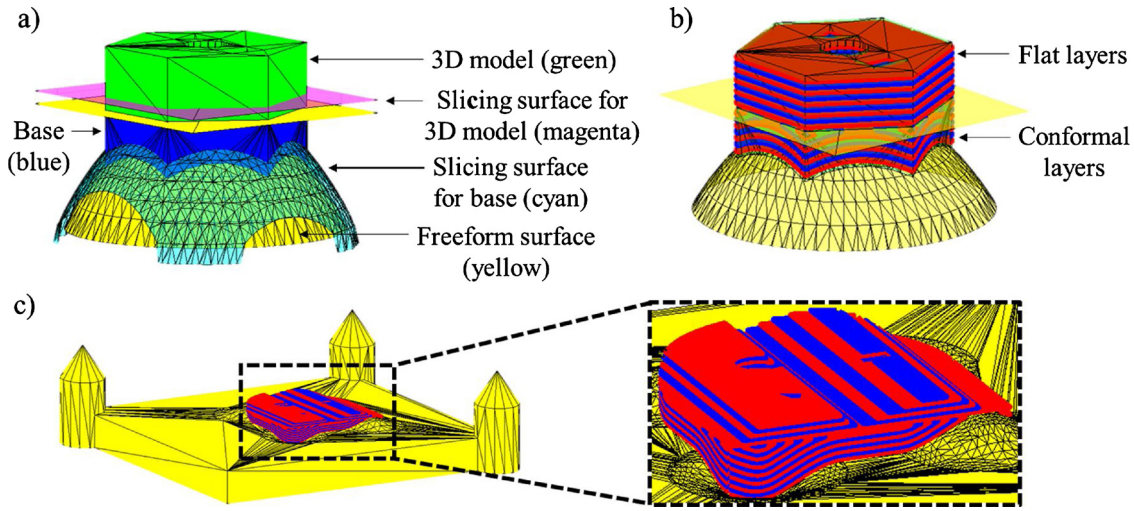

Fig. 7. Visual representation of 3D slicing of the base and the 3D model using the hybrid slicing method: a) 3D view of the base (in blue), the conformal slicing surface for the base (in cyan), the 3D model (in green) and the planar 2D slicing surface for the 3D model (in magenta), yellow plane represents the interface between the base and the top part; b) 3D view of the conformal layers of the base and the flat layers of the 3D model; and c) Hybrid 3D slicing of the printed part and base shown in Fig. 3e. (For interpretation of the references to colour in this figure legend, the reader is referred to the web version of this article.)

created to fill the gap between them (Fig. 3e). In this example, the base and the printed part were sliced using the hybrid slicing method (as outlined in Section 2.2), where the base was sliced conformably and the printed part was sliced conventionally (planar slicing), as shown in Fig. 7c.

4. Results and discussion

This study demonstrates the capability of the proposed algorithm to automatically generate a toolpath for conformal 3D layers in order to build 3D structures on freeform surfaces. Experiments for two 3D slicing and printing methods (fully conformal and hybrid) were performed successfully.

Fig. 9 shows the results for the conformal 3D printing of the hexagonal and UA models shown in Fig. 2a, b and d, respectively. These two parts were sliced using the fully conformal slicing method (presented in Fig. 6b and d).

The result in Fig. 10 shows the hybrid 3D printing of the parts shown in Fig. 3b and e, according to the hybrid slicing method shown in Fig. 7b and c, respectively. From these results, the high performance of the proposed algorithm for printing different geometrical shapes on different freeform substrates (a sphere and an arbitrary flat surface containing convex domes and concave craters) can clearly be seen.

The printing material with thixotropic demonstrated great performance in terms of maintaining the filament shape with respect to the dynamic change in the angle between the nozzle tip and the freeform substrate. This material is also shown to be capable of achieving a gel-like state that can maintain the shape of the 3D printed part without collapsing after printing.

One significant phenomenon resulting from 3D printing on a conformal surface with a three-axis Cartesian system is the lack of consistency in the filament width. This issue occurs when the angle

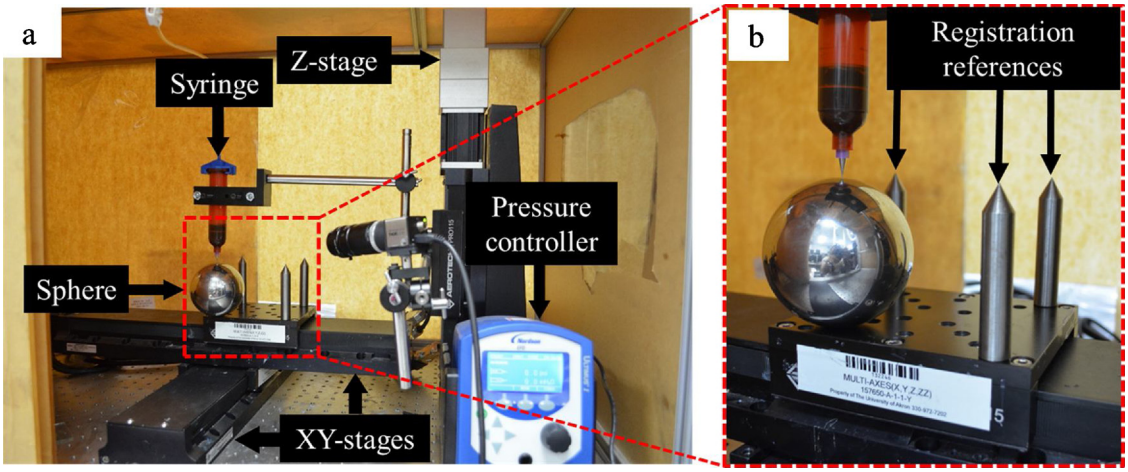

Fig. 8. Developed direct-print system, a) Setup of system components, b) Setup used to determine the origin point on the sphere to use for locating points on the surface of the substrate.

between the printing nozzle and the freeform substrate changes as the printing proceeds, and it results in the phenomena of filament leading and lagging (Fig. 11a, c). The authors have investigated and resolved this issue in order to achieve a constant filament width during printing on a freeform substrate, as described in a previous publication [39].

Based on the experimental results, the proposed algorithm developed in this study is expected to be applicable for Cartesian systems with both three degrees of freedom (translation) and five degrees of freedom when adding rotation around *x*-axis and the *y*-axis. In this study, the 3D printing system consists of three translating axes (*x*-, *y*-, and *z*-axis), which limits the nozzle tip to three degrees of freedom. This limited movement of the nozzle tip leads to a maximum inclination angle between the nozzle and the freeform substrate of 45°.

Fig. 12 shows the results of a third experiment conducted as part of this study that involved printing circular lines on a freeform surface. The lines were designed to be printed at various inclination angles between the nozzle (on the *z*-axis) and a spherical freeform substrate, as shown in Fig. 12a. From Fig. 12b, it can be noticed that the lines were successfully printed on the sphere. However, after printing, the ink began to flow downward as the force of gravity overcame the filament–substrate adhesion force (as can be seen in the close-up photo in Fig. 12c).

5. Conclusions

Conformal 3D printing has been used for different applications that involve customization or repairs, such as the printing of customized electrical circuits on freeform surfaces, as well as printing to repair worn-out surfaces such as the treads on vehicle tires. Successful conformal 3D printing mainly relies on proper nozzle toolpath generation and printing accuracy. In this work, an algorithm was presented in order to slice 3D structures and generate toolpath data points of conformal layers to be 3D printed onto freeform surfaces. In order to build the desired 3D structure on a freeform substrate, the bottom of the 3D structure must fit the freeform substrate without any gaps. Therefore, in the case of a mis-match between the freeform substrate and the 3D model for some applications, a new part (called a *base*) must be generated to connect the two. In order to slice the 3D structure and extract the printing toolpath, the freeform surface is used as a slicing surface after offsetting it with an amount equal to gap the height. The toolpath data points for each layer consists of perimeters and infill data points. The perimeter data points are extracted from the intersection line between the 3D model and the slicing surface, while the infill data points are the result of the projection of a 2D pattern on the slicing surface. To avoid passing through internal features of each layer during printing,

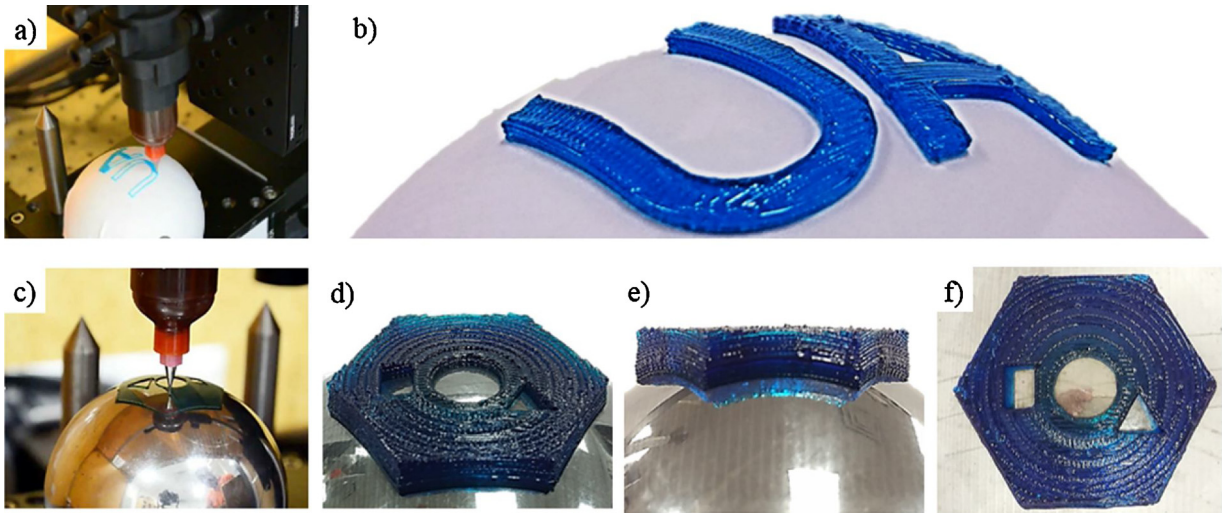

Fig. 9. 3D printing of a UA and a hexagonal-shaped models with internal features on a sphere-shaped substrate using the fully conformal slicing method: a) 3D printing of the first layer of the UA part, b) The complete print of the UA part, c) 3D printing of the first layer of the hexagonal-shaped part, d) The complete print of the hexagonal-shaped part, e) Side view of the printed hexagonal-shaped part, and f) Top view of the printed hexagonal-shaped part.

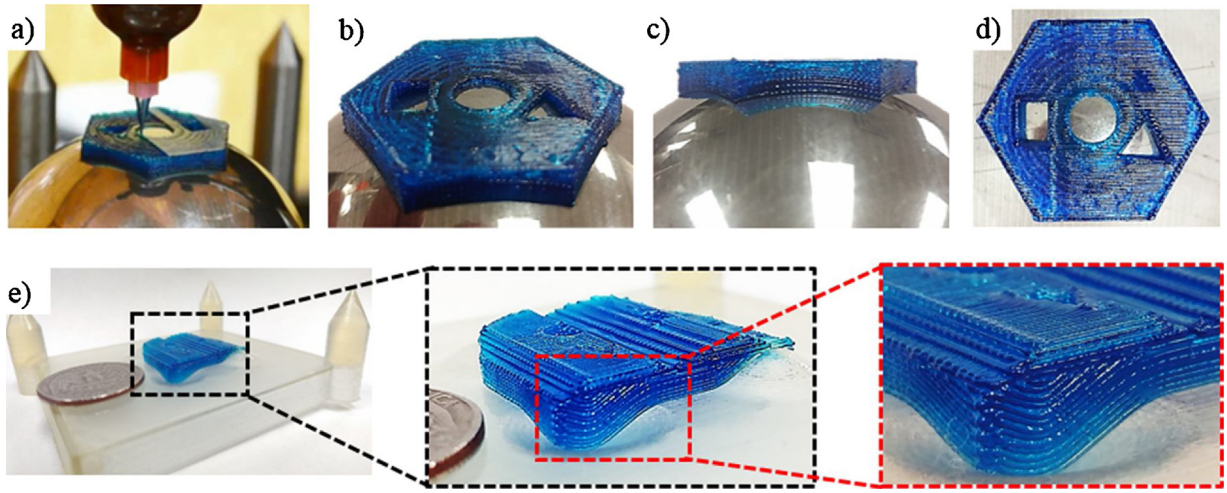

Fig. 10. 3D printing of a hexagonal-shaped and an arbitrary-shaped parts with internal features on a sphere-shaped substrate the hybrid slicing method: a) 3D printing of the first layer of the hexagonal part on the top of the base, b) The complete hybrid 3D print of the hexagonal-shaped part, c) Side view of the printed hexagonal-shaped part, d) Top view of the printed hexagonal-shaped part, and e) Hybrid 3D print of the part shown in Fig. 3e.

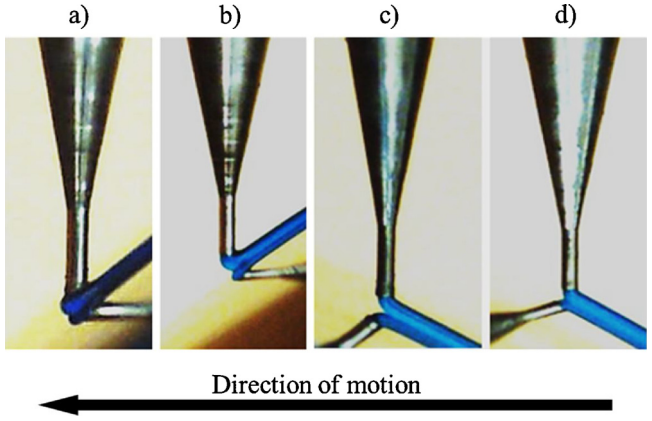

Fig. 11. Leading/lagging phenomena in the 3D printing process, a) Leading when no algorithm was used, b) Leading when using the algorithm developed in a prior study [39], c) Lagging when no algorithm was used, and d) Lagging when using the algorithm developed in a prior study [39].

the data points for the infill toolpath were divided into segments and combined with the perimeter data points for each layer. Since different applications can require different slicing methods, two 3D slicing methods were presented and discussed in this work. In the first method (fully conformal slicing), both the base and the 3D model are sliced conformably as if they are a single part, and they are sliced according to the shape of the freeform substrate. In the second method (hybrid slicing), the base is sliced conformably according to the shape of the freeform substrate, the 3D model is sliced using conventional planar slicing, and the base and substrate are combined into a single G-code file to enable them to be built as a single part. In this study, a printing ink having a specific thixotropic behavior was developed for use in this process. Different 3D structures were designed and were 3D printed on freeform substrates as a proof of the algorithm efficacy using a Cartesian coordinate system with three degrees of freedom. The 3D structures were built using both slicing methods, as mentioned previously. In addition, 45° was identified as the maximum inclination angle between the nozzle and the freeform substrate when using a Cartesian system with only three degrees of freedom. In order to overcome the limitation imposed by the angle of inclination, the proposed algorithm will be extended so that it will be applicable for printing systems with five degrees of freedom by adding rotation around the *x*-axis and *y*-axis. In addition, changes in mechanical properties for a part manufactured by the suggested method will be investigated in future.

Conflict of interest

One or more of the authors of this article are a part of the Editorial Board of the journal. To avoid a potential conflict of interest, the responsibility for the editorial and peer-review process of this article lies with a different editor. Furthermore, the authors of this article were removed from the peer review process and had no, and will not have, any access to confidential information related to the editorial process of this article.

Acknowledgements

This work was supported by research grants from Center for Tire

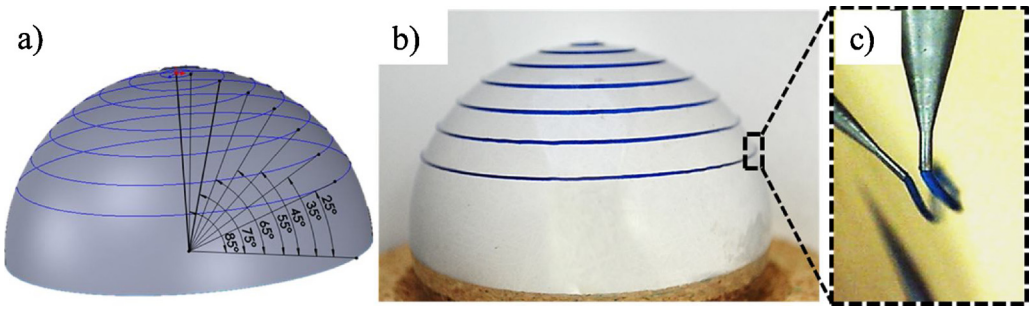

Fig. 12. Direct printing of lines using different angles between the nozzle (in a vertical orientation) and the freeform substrate: a) CAD design showing inclination angles used to print the desired lines (with lines indicated in blue); b) Printed lines on the spherical freeform surface; and c) Ink material flowing downward due to the high inclination angle between the nozzle and the substrate. (For interpretation of the references to colour in this figure legend, the reader is referred to the web version of this article.)

Research (CenTiRe) and Brain Pool Program through the National Research Foundation of Korea (NRF) funded by the Ministry of Science and ICT (2019H1D3A2A01059934). Dr. Faez Alkadi received a full scholarship in completing this work which was supported by Jazan University through Saudi Arabian Cultural Mission (SACM).

Appendix A. Supplementary data

Supplementary material related to this article can be found, in the online version, at doi:https://doi.org/10.1016/j.addma.2019.100975.

References

[1] K.V. Wong, A. Hernandez, A review of additive manufacturing, ISRN Mech. Eng. 2012 (2012).
[2] D.T. Pham, R.S. Gault, A comparison of rapid prototyping technologies, Int. J. Mach. Tools Manuf. 38 (10–11) (1998) 1257–1287.
[3] B.N. Turner, R. Strong, S.A. Gold, A review of melt extrusion additive manufacturing processes: I. Process design and modeling, Rapid Prototyp. J. 20 (3) (2014) 192–204.
[4] J.A. Lewis, G.M. Gratson, Direct writing in three dimensions, Mater. Today 7 (7–8) (2004) 32–39.
[5] B.Y. Ahn, et al., Omnidirectional printing of flexible, stretchable, and spanning silver microelectrodes, Science 323 (5921) (2009) 1590–1593.
[6] K. Sun, et al., 3D printing of interdigitated Li-Ion microbattery architectures, Adv. Mater. 25 (September 33) (2013) 4539–4543.
[7] M. Vatani, et al., Direct-write stretchable sensors using single-walled carbon nanotube/polymer matrix, J. Electron. Packag. 135 (1) (2013) 11009.
[8] M. Vatani, E.D. Engeberg, J.W. Choi, Force and slip detection with direct-write compliant tactile sensors using multi-walled carbon nanotube/polymer composites, Sens. Actuators A-Phys. 195 (June) (2013) 90–97.
[9] J.-W. Choi, M. Vatani, E.D. Engeberg, Direct-Write of Multi-Layer Tactile Sensors, (2019), pp. 164–168.
[10] C.P. Jiang, J.R. Huang, M.F. Hsieh, Fabrication of synthesized PCL-PEG-PCL tissue engineering scaffolds using an air pressure-aided deposition system, Rapid Prototyp. J. 17 (4) (2011) 288–297.
[11] S. Khalil, J. Nam, W. Sun, Multi-nozzle deposition for construction of 3D biopolymer tissue scaffolds, Rapid Prototyp. J. 11 (1) (2005) 9–17.
[12] E. Malone, H. Lipson, Asme, Multi-material freeform fabrication of active systems, Proceedings of the 9th Biennial Conference on Engineering Systems Design and Analysis 1 (2008) 345–353 2009.
[13] V. Mironov, et al., Organ printing: computer-aided jet-based 3D tissue engineering, Trends Biotechnol. 21 (April 4) (2003) 157–161.
[14] L. Geng, et al., Direct writing of chitosan scaffolds using a robotic system, Rapid Prototyp. J. 11 (2) (2005) 90–97.
[15] S. Ghosh, et al., Direct-write assembly of microperiodic silk fibroin scaffolds for tissue engineering applications, Adv. Funct. Mater. 18 (July 13) (2008) 1883–1889.
[16] R.A. Barry, et al., Direct-write assembly of 3D hydrogel scaffolds for guided cell growth, Adv. Mater. 21 (June 23) (2009) pp. 2407-+.
[17] B.Y. Ahn, et al., Direct-write assembly of microperiodic planar and spanning ITO microelectrodes, Chem. Commun. 46 (38) (2010) 7118–7120.
[18] S. Singamneni, et al., Modeling and evaluation of curved layer fused deposition, J. Mater. Process. Technol. 212 (January 1) (2012) 27–35.
[19] D. Chakraborty, B.A. Reddy, A.R. Choudhury, Extruder path generation for curved layer fused deposition modeling, Comput. Des. 40 (February 2) (2008) 235–243.
[20] R.J. Allen, R.S. Trask, An experimental demonstration of effective Curved Layer Fused Filament Fabrication utilising a parallel deposition robot, Addit. Manuf. 8 (2015) 78–87.
[21] T. Llewellyn-Jones, R. Allen, R. Trask, Curved layer fused filament fabrication using automated toolpath generation, 3D Print. Addit. Manuf. 3 (December 4) (2016) 236–243.
[22] J.J. Adams, et al., Conformal printing of electrically small antennas on three-dimensional surfaces, Adv. Mater. 23 (March 11) (2011) 1335–1340.
[23] B. Huang, S. Singamneni, Alternate slicing and deposition strategies for fused deposition modelling of light curved parts, J. Achiev. Mater. Manuf. Eng. 55 (2) (2012) 511–517.
[24] D.W. Hutmacher, et al., Mechanical properties and cell cultural response of polycaprolactone scaffolds designed and fabricated via fused deposition modeling, J. Biomed. Mater. Res. 55 (May 2) (2001) 203–216.
[25] A. Boschetto, L. Bottini, Accuracy prediction in fused deposition modeling, Int. J. Adv. Manuf. Technol. 73 (5–8) (2014) 913–928.
[26] J. Tyberg, J.H. Bohn, FDM systems and local adaptive slicing, Mater. Des. 20 (June 2–3) (1999) 77–82.
[27] C. Bellehumeur, et al., Modeling of bond formation between polymer filaments in the fused deposition modeling process, J. Manuf. Process. 6 (2) (2004) 170–178.
[28] X.B. Le, et al., Mechanical property testing and analysis of 3D printing objects, Proceedings of the Asme International Mechanical Engineering Congress and Exposition, 2016 2 (2017).
[29] A. Bellini, S. Guceri, Mechanical characterization of parts fabricated using fused deposition modeling, Rapid Prototyp. J. 9 (4) (2003) 252–264.
[30] P.M. Pandey, N.V. Reddy, S.G. Dhande, Improvement of surface finish by staircase machining in fused deposition modeling, J. Mater. Process. Technol. 132 (January 1–3) (2003) 323–331.
[31] A. Boschetto, L. Bottini, Design for manufacturing of surfaces to improve accuracy in Fused Deposition Modeling, Robot. Comput. Manuf. 37 (2016) 103–114.
[32] D. Ahn, et al., Representation of surface roughness in fused deposition modeling, J. Mater. Process. Technol. 209 (August 15–16) (2009) 5593–5600.
[33] J. Wang, et al., A novel approach to improve mechanical properties of parts fabricated by fused deposition modeling, Mater. Des. 105 (2016) 152–159.
[34] N. Bausch, et al., 3D printing onto unknown uneven surfaces, IFAC Papersonline 49 (21) (2016) 583–590.
[35] Y. Jin, et al., Modeling and process planning for curved layer fused deposition, Int. J. Adv. Manuf. Technol. 91 (July 1–4) (2017) 273–285.
[36] B.G. Compton, J.A. Lewis, 3D-printing of lightweight cellular composites, Adv. Mater. 26 (34) (2014) 5930–5935.
[37] M. Vatani, E.D. Engeberg, J.-W. Choi, Conformal direct-print of piezoresistive polymer/nanocomposites for compliant multi-layer tactile sensors, Addit. Manuf. 7 (2015) 73–82.
[38] R.B. Rusu, S. Cousins, 3d is Here: Point Cloud Library (pcl). (2019), pp. 1–4.
[39] M. Vatani, F. Alkadi, J.-W. Choi, Algorithm to reduce leading and lagging in conformal direct-print, J. Manuf. Sci. Eng. 140 (10) (2018) 101014.
[40] T. Möller, A fast triangle-triangle intersection test, J. Graph. Tools 2 (2) (1997) 25–30.
[41] T. Möller, B. Trumbore, Fast, Minimum Storage Ray/Triangle Intersection, p. 7 (2019).